Supporting Information: Understanding excited state properties of host materials in OLEDs: simulation of absorption spectrum of amorphous 4,4-bis(carbazol-9-yl)-2,2-biphenyl (CBP)

Samaneh Inanlou[b], Rodrigo Cortés-Mejía[b], Ali Deniz Özdemir[c], Sebastian Höfener[b], Wim Klopper[b,c], Wolfgang Wenzel[c], Weiwei Xie[a*], Marcus Elstner[b,d]

[a] *Key Laboratory of Advanced Energy Materials Chemistry (Ministry of Education), Renewable Energy Conversion and Storage Center, College of Chemistry, Nankai University, Tianjin, 300071, China*

[b] *Institute of Physical Chemistry, Karlsruhe Institute of Technology (KIT), 76131 Karlsruhe, Germany*

[c] *Institute of Nanotechnology, Karlsruhe Institute of Technology (KIT), Hermann-von-Helmholtz-Platz 1, 76344 Eggenstein-Leopoldshafen, Germany*

[d] *Institute of Biological Interfaces (IBG-2), Karlsruhe Institute of Technology (KIT), Hermann-von-Helmholtz-Platz 1, 76344 Eggenstein-Leopoldshafen, Germany*

S-1. Force field reparameterization

This section presents the reparametrization of dihedral angles which is restricted to the proper and improper dihedral angles. The reason behind this is that the excitation energies and consequently the absorption bands can be affected by the dihedral angles. Force-field reparameterization can be performed by matching the quantum mechanical potential energy surface (PES) scans with the corresponding force-field based scans. To reparametrize the parameters of the general AMBER force field (GAFF), three sets of parameters are considered: side/central dihedral angles (α and β) and improper dihedral angle ($\square$) (Fig. 1). The potential energy scans for the corresponding angles are performed using density functional theory (DFT) methods (ωB97XD functional) and 6-311g+(d,p) basis set. The potential energies are obtained from rotational scans where the corresponding angle is fixed (e.g., α in Fig. 1). Throughout the calculations, all the geometrical parameters are simultaneously relaxed while their respective dihedral angles vary from 0° to 180° for side and central angles and from 0° to 30° for improper angles in steps of 5°. The difference between DFT and force-field based energies is then fitted, yielding the parameterization constants of the dihedral using the GAUSSIAN package, and all force-field computations are carried out using the GROMACS package. For the proper and improper dihedral angles, the periodic and harmonic functions are used as per equations (1) and (2), respectively:

$$V_d(\phi_{ijkl}) = k_\phi\left(1 + \cos\left(n\phi - \phi_s\right)\right) \tag{1}$$

$$V_{id}(\xi_{ijkl}) = \frac{1}{2}k_\xi(\xi_{ijkl} - \xi_0)^2 \tag{2}$$

After fitting, the coefficients of the periodic and harmonic functions (k) for side (α), central (β) and improper (γ) dihedral angles are 4.25, 2.883 and 11.88 respectively. The results are shown in Fig. S1 (b). For the side angle, the DFT scan shows that the torsional potential has 2 minima when $\alpha \approx 60°$ and another local minimum at $\alpha \approx 120°$. The geometry at $\alpha \approx 90°$ has a barrier to planarity of about 3 kcal/mol. Concerning the central angle, the rotational barrier at 0° and 90° of biphenyl originate from two factors, the interaction between π orbitals of the benzene rings, which makes biphenyl planar and repulsion between ortho-hydrogen atoms to makes the molecule to rotated the geometry with $\beta \approx 40°$ or 140° [1]. The barrier at $\beta = 90°$ is about 6 kJ/mol. For the improper angle, as the out-of-plane angle decreases, the electronic conjugation increases. Therefore, the planar geometry ($\gamma \approx 0$ or 180°) has an extended electronic conjugation of π-electrons which facilitates extended conjugation of CBP. The rotational barrier at $\gamma \approx 30°$ or 150°, is a result of breakage of the electronic conjugation.
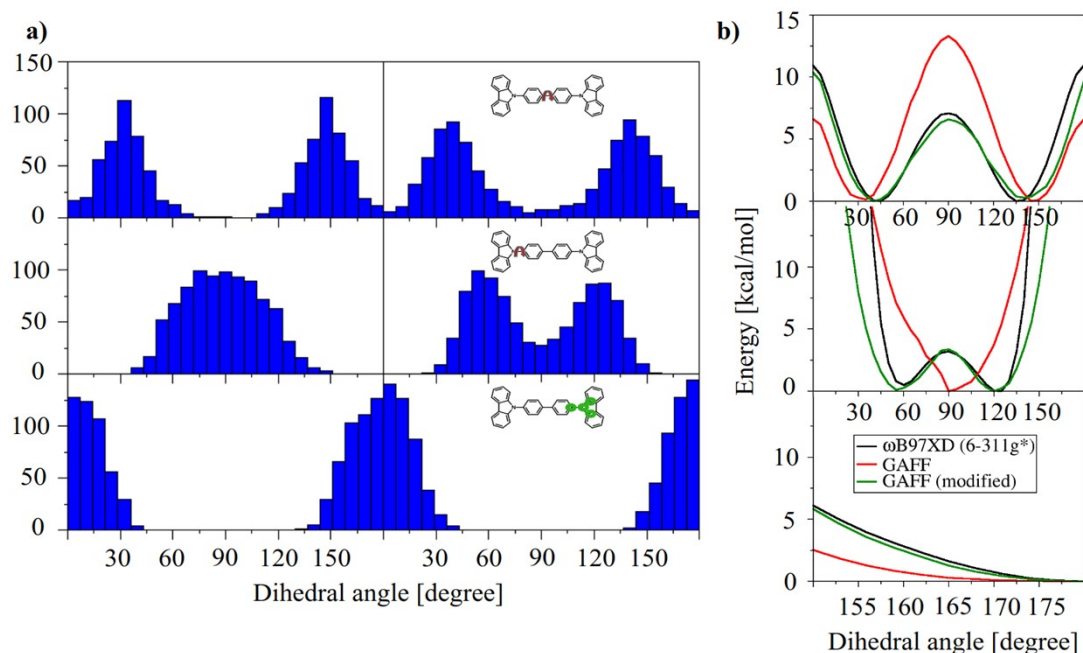

Figure S1. a) Distributions of central (upper panel), and side (center panel) and improper (lower panel) angles obtained by MD sampling using original GAFF and reparameterized GAFF force fields. b) Potential energy

relaxed scans along central (upper panel), and side (center panel) and improper (lower panel) angles using ωB97XD/6-311g+(d,p) (black) and original GAFF (red) and reparameterized GAFF (green).

S-2. Bond length alternation and excitation energies

The dependence of optical properties of a π-Conjugated system on the ground state BLA is performed by analyzing the effects of using various quantum chemistry methods for geometry optimization. BLA is determined by the difference between the length of single- and double-bonds along the conjugation chain. (see red mark in Fig. 1 (b) in the main text). The calculated bond lengths and BLAs are listed in Table S1

Table. S1 Bond lengths and bond-length alternation (BLA) for the CBP molecule optimized by various quantum chemistry methods.

	Bond Length [Å]							BLA
	$C_1=C_2$	C_2-C_3	$C_3=C_4$	C_4-C_5	$C_5=C_6$	C_6-C_7	$C_7=C_8$	
FF	1.410	1.400	1.399	1.514	1.393	1.402	1.410	0.036
HF	1.388	1.380	1.382	1.488	1.382	1.380	1.389	0.031
ωB97XD	1.393	1.383	1.389	1.480	1.389	1.383	1.393	0.025
B3LYP	1.399	1.387	1.394	1.480	1.394	1.387	1.399	0.021
PBE	1.395	1.383	1.391	1.474	1.391	1.383	1.395	0.020
MP2	1.397	1.390	1.402	1.471	1.402	1.390	1.397	0.017
DFTB	1.408	1.392	1.408	1.484	1.408	1.392	1.408	0.014

Table. S2 Vertical excitation energies (eV) of fully optimized geometries in vacuum using various quantum chemistry methods.

	FF	MP2	HF	ωB97XD	B3LYP	PBE	DFTB3
HF/CIS	4.82	4.79	5.06	4.97	4.90	4.84	4.50
ωB97XD	4.25	4.28	4.42	4.35	4.32	4.33	4.11
TD-LC-DFTB	4.01	3.98	4.26	4.10	4.05	4.04	3.83
CC2	3.89	3.97	4.11	4.04	4.01	4.02	3.85
ADC(2)	3.89	3.95	4.09	4.01	3.98	4.00	3.84
GW-BSE	3.85	3.93	4.09	4.00	3.97	3.98	3.86
PBE	3.72	3.66	3.80	3.75	3.69	3.68	3.53
B3LYP	3.58	3.51	3.61	3.59	3.53	3.53	3.40
TD-DFTB	3.11	3.03	3.01	3.11	3.03	3.07	2.97

Table. S3 Vertical excitation energies (eV) of optimized CBP geometries in vacuum with constraint dihedral angles at 45°, 60° and 0° for α, β and □.

	FF	HF	ωB97XD	B3LYP	PBE
ADC(2)	5.195	5.360	5.294	5.254	5.269
HF/CIS	4.960	5.063	5.066	5.023	5.052
ωB97XD	4.290	4.453	4.395	4.363	4.380
B3LYP	3.638	3.669	3.622	3.588	3.601
PBE	3.790	3.833	3.784	3.749	3.761
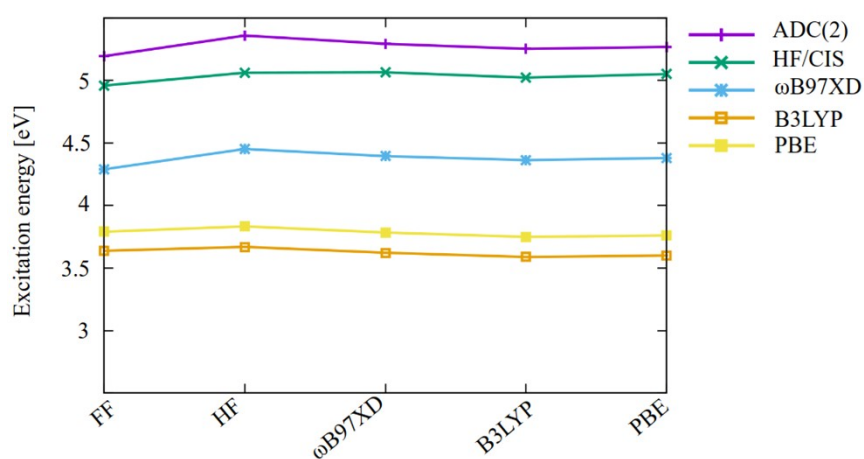
Figure S2. Excitation energies (eV) for different optimized geometries with constraint dihedral angles.

S-3. Absorption spectra in gas phase

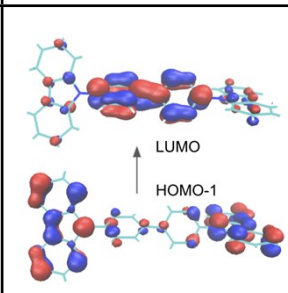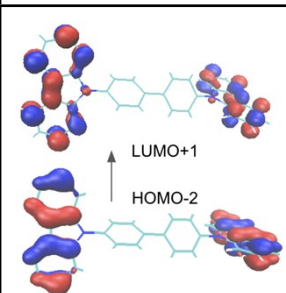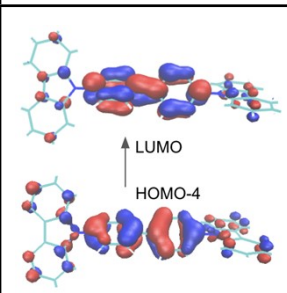**Table. S4** Electron transitions relevant to HOMO-n (n=1,2,4) obtained by LC-DFTB.

Excitation energy /oscillator strength	ΔE = 4.49 eV f = 0.00	ΔE = 4.54 eV f = 0.02	ΔE = 5.47 eV f = 0.16
Transition Orbitals			

Table. S5 Excitation energies (in eV) of the lowest-energy peak in the gas-phase static absorption spectra for side (α) and central (β) dihedral angles from 0° to 90° in 10 degrees obtained using TD-LC-DFTB and GW-BSE (shown in parentheses).

	0°	10°	20°	30°	40°	50°	60°	70°	80°	90°
α	3.96 (3.86)	3.96 (3.87)	3.97 (3.90)	3.98 (3.94)	4.00 (3.97)	4.02 (3.98)	4.05 (3.99)	4.07 (4.00)	4.09 (4.02)	4.10 (4.01)
β	3.91 (3.92)	3.92 (3.96)	3.95 (3.98)	3.99 (3.98)	4.04 (3.99)	4.09 (3.99)	4.12 (3.97)	4.14 (3.98)	4.15 (3.98)	4.15 (3.98)

Table. S6 LC-DFTB Kohn−Sham orbitals involved in the excitation of the lowest-energy peak for side (α) and central (β) dihedral angles at 0° and 90°.
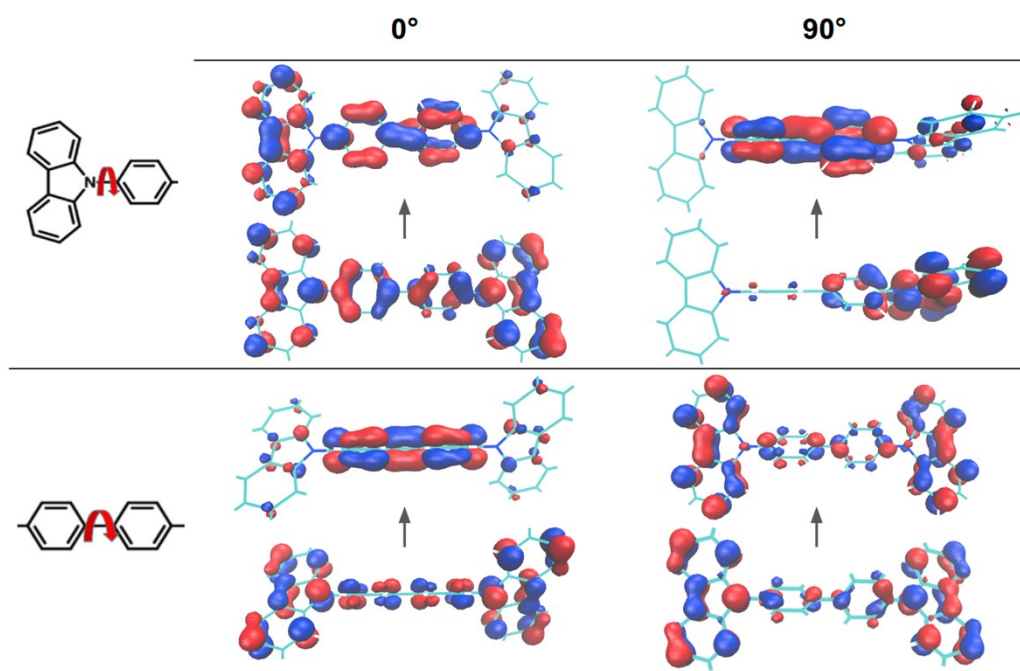
S-4. Correlation between snapshot at t=0 and t=1 ps.

Figure S3 shows the time-dependent velocity autocorrelation function Z(t). At 1 ps, the velocity autocorrelation function is less than 0.1, which indicates there is minor correlation between the snapshot at t = 1ps and the snapshot at t=0. Therefore, the snapshots used for structure sampling are approximately uncorrelated.
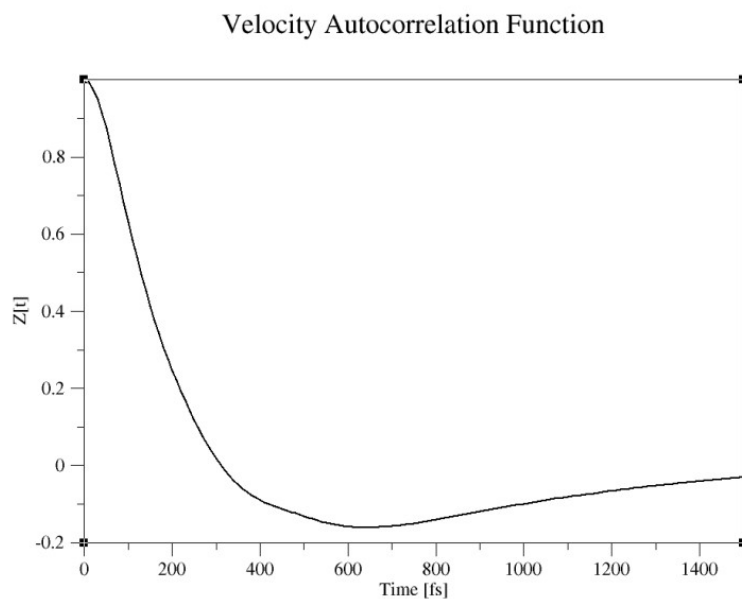

Figure S3 Velocity autocorrelation functions

S-5. The effect of electrostatic interactions

Fig. S4 shows the absorption spectrum of 1 MD-snapshot containing 5000 molecules with and without electrostatic interactions. The electrostatic interactions were represented by surrounding point charges. The absorption spectra are similar, indicating that the electrostatic interactions have minor effects on the absorption spectrum.
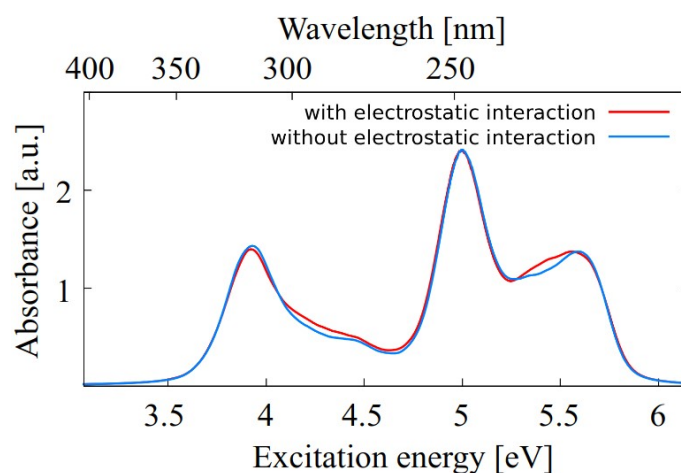

Figure S4. Comparison of absorption spectra for an ensemble-snapshot of 5000 molecules with and without considering electrostatic effect on excitation energy calculations. The electrostatic effects were considered by the point charge scheme.

This finding is not unexpected, since the environment is quite apolar. To understand this in detail, the references to other QM/MM calculations of embedded chromophores may be instructive. In a recent work [2], we computed the excitation energies of retinal and chlorophylls in their respective protein environments. The response to the environment is very different: While retinal excitation e nergies are highly tunable by the protein electrostatic environment, the excitation energies of chlorophylls are much less sensitive. This depends on (i) the electronic structure of the pigment and (ii) the polarity of the environment. Therefore, also in highly polar protein environments, the effects of color shifts can be very diverse. The protein environment in retinal proteins is specifically organized, in order to promote certain color shifts of the chromophore, which is particularly important for the process of vision: Here, different protein environments enable color shifts over 300 nm in order to absorb in the different wave-length regimes of visible light. In case of CBP, in contrast, this effect is very small, as expected, since the surrounding molecules are (i) quite apolar and (ii) randomly oriented.

Please note, however, that our recent study showed [2], that some LC-DFT methods, including LC-DFT, slightly underestimate the effect of electrostatic tuning. This means, these methods should be applied to systems with care, where these effects are large, like retinal proteins. In systems, where this effect is small, this does not lead to a large error in the absorption spectra. In the case of chlorophylls in light-harvesting complexes, the main effects are exciton couplings, in the case of CBP, the main effects are structural changes, which are both covered quite well by LC-DFTB.

S-6. Convergence test for time-series sampling with the number of individual molecules sampled in the supercell
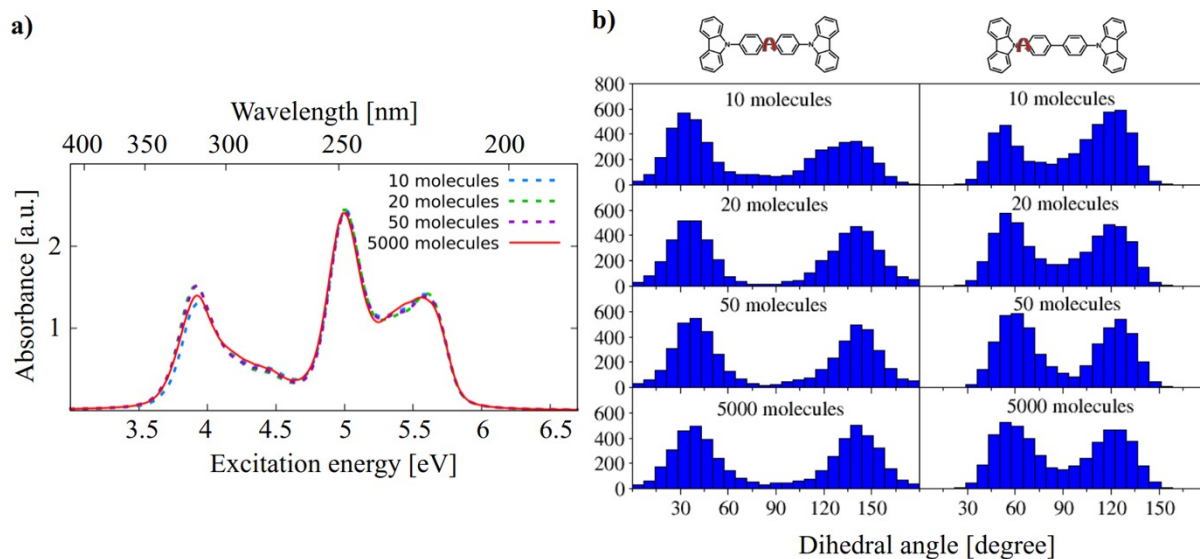
a)

b)

Figure. S5 Convergence of the absorption spectra (a) and dihedral angles with the number of individual molecules sampled in the supercell.

References

[1] S. Arulmozhiraja and T. Fujii, Torsional barrier, ionization potential, and electron affinity of biphenyl—A theoretical study, J. Chem. Phys. 115, 10589 (2001).

[2] B. M. Bold, M. Sokolov, S. Maity, M. Wanko, P. M. Dohmen, J. J. Kranz, U. Kleinekathofer, S. Hofener, and M. Elstner, Benchmark and Performance of Long-Range Corrected Time-Dependent Density Functional Tight Binding (LC-TD-DFTB) on Rhodopsins and Light-Harvesting Complexes, Phys. Chem. Chem. Phys., (2020), 22, 10500.